Ind. J. Pharm. Edu. Res., 2026; 60(4):1787-1800.
https://www.ijper.org

Original Article

Isolation and Mechanistic Exploration of FS-1: A Pro-Apoptotic Protein from *Gloydius brevicaudus* Venom in Tumor Cells

Jianguo Hu*, Hongxia Guo, Chuang Wang, Yun Chen

Faculty of Modern Health Care, Anhui Sanlian University, Hefei, Anhui, CHINA.

ABSTRACT

Background/Objectives: Components potentially inducing tumor cell apoptosis were isolated from *Gloydius brevicaudus* venom, and their apoptotic mechanisms were investigated. **Materials and Methods:** The lyophilized venom was fractionated using anion exchange chromatography (DEAE-Sepharose Fast Flow), cation exchange chromatography (Sp-Sepharose Fast Flow), and gel filtration chromatography (Sephadex G-75), leading to the isolation of a component (FS-1) that appeared to inhibit tumor proliferation. SDS-PAGE analysis indicated a single band with an approximate molecular weight of 25 kDa. **Results:** FS-1 was observed to inhibit the proliferation of HeLa and Hep G2 cell lines in a dose-dependent manner. A time-dependent decrease in IC_{50} values was noted, with the most pronounced effect observed at 48 hr. Evidence suggested FS-1 induced tumor cell apoptosis: fluorescence staining indicated PS externalization from the inner to the outer leaflet of the cell membrane after 6 hr of treatment. ELISA experiments detected an increase in BAD expression at 12 hr. By 24 hr, an increase in cytosolic Cyt C concentration was observed, accompanied by a decrease in mitochondrial Cyt C concentration. Data suggested enhanced expression of BAX, while reduced expression of Bcl-2 and Bcl-xl was detected. Fluorescence staining indicated the opening of the mitochondrial MPTP. At 36 hr, increased activities of caspase-8 and caspase-9 were measured. By 48 hr, enhanced activities of caspase-3 and caspase-6 were also detected, and DNA damage was observed via agarose gel electrophoresis. Western blot analysis of Bcl-2, Bcl-xl, caspase-3, and caspase-6 supported these observations. Additionally, AIF was detected in the cytoplasm, showing increased concentration and the presence of cleaved bands. **Conclusion:** Collectively, these findings suggest the successful isolation of anti-tumor protein from *Gloydius brevicaudus* venom that induces tumor cell apoptosis, mediated through mechanisms involving mitochondrial dysfunction and caspase activation.

Keywords: *Gloydius brevicaudus*, Venom, Apoptosis, Hep G2, HeLa.

Correspondence:
Dr. Jianguo Hu
Faculty of Modern Health Care, Anhui Sanlian University, Hefei, Anhui-230601, CHINA.
Email: erhu1999@126.com

Received: 03-04-2026;
Revised: 29-06-2026;
Accepted: 13-08-2026.

INTRODUCTION

Snake venom is a complex biological fluid secreted by the venom glands of snakes, comprising a diverse array of toxins. Its primary constituents are proteins, which exhibit a broad spectrum of physiological activities. The primary biological roles of snake venom include prey immobilization, initiation of digestive processes, and serving as a defense mechanism.[1] Research on snake venom is of significant biomedical interest, contributing to the understanding of disease mechanisms, the development of diagnostic tools, and the discovery of novel therapeutic agents. Notably, snake venom-derived coagulation and fibrinolytic enzymes have been widely investigated for clinical applications, including those derived from *Gloydius brevicaudus* and Deinagkistrodon acutus.[2,3]

A key focus in recent snake venom research is the identification of anti-tumor components and elucidation of their mechanisms of action.[4] Several studies have provided valuable insights into this area. For instance, Xiong Yan *et al*., reported that *Deinagkistrodon acutus* venom exhibited inhibitory effects on human ovarian cancer A2780 cells.[5] Similarly, Ebrahim *et al*., demonstrated that Naja naja oxiana venom effectively inhibited the proliferation of Human Breast Cancer Cells (MCF-7), liver cancer cells (Hep G2), and prostate cancer cells (DU145).[6] Additionally, Moridikia *et al*., found that *Viper alatifii* venom significantly suppressed Hep G2 cell activity, while Gomes *et al*., identified a fraction (drCT-1) from *Daboia russelli russelli* venom with potent anti-leukemic properties.[7,8]

DOI: 10.5530/ijper.20262119

Furthermore, Duan Tao *et al.*, isolated a cytotoxin (I3H3) from *Deinagkistrodon acutus* venom that inhibited human nasopharyngeal carcinoma (KB), Gastric Carcinoma (BGC), and lung cancer (A549) cell lines.[9] Three small peptide molecules-pyroglutamyl-lysinyl-tryptophan, pyroglutamyl-menthyl-tryptophan, and pyroglutamyl-glutamy l-tryptophan-purified from *Deinagkistrodon acutus* venom were found to exhibit strong inhibitory and cytotoxic effects against various cancer cell lines, including Gastric Cancer (BGC-283), breast cancer (MDA-MB-231), lung cancer (A549), and hepatocellular Carcinoma (SMMC-7721).[10] Additionally, Xu *et al.*, identified an acidic protein, AAVC-1, from *Deinagkistrodon acutus* venom, which significantly inhibited A549 cells and induced apoptosis.[11] Li *et al.*, also isolated an anti-metastatic component from *Gloydius brevicaudus* venom that inhibited breast cancer metastasis.[12]

Despite these advances, research on the anti-tumor properties of *Gloydius brevicaudus* venom remains limited. In this study, we employed ion-exchange chromatography and gel filtration chromatography to isolate active proteins from *Gloydius brevicaudus* venom and investigated their mechanisms of inducing apoptosis in tumor cells.

MATERIALS AND METHODS

Preparation of *Gloydius brevicaudus* Venom Extract

The freeze-dried *Gloydius brevicaudus* venom (Batch No: 20190703) was obtained from Huangshan Snake Garden (Huangshan City, Anhui Province, China) and stored at 4°C.

For experimental use, 1 g venom powder was dissolved in 10 mL of Tris-HCl buffer (pH 8.0, 10mM) at 4°C. After centrifugation at 10,000 rpm for 15 min at 4°C, the supernatant was collected.

Human Tumor Cell Lines and Culture Conditions

The HeLa and Hep G2 cell lines were obtained from Wuhan Purosai Life Science and Technology Co., Ltd., China. MEM medium was sourced from the same supplier, while Fetal Bovine Serum (FBS) was purchased from Hangzhou Four Seasons Green Company, China.

HeLa/Hep G2 cells were cultured in MEM + 10% FBS + 1% penicillin-streptomycin. Cells were passaged at 80% confluency (1:3 split ratio) and used within 15 passages. Cells were maintained at 37°C in a humidified atmosphere with 5% CO_2. Cells were passaged at 80% confluency using 0.25% trypsin-EDTA. No serum starvation was applied during the culture process.

Isolation of *Gloydius brevicaudus* Venom Proteins

The venom protein purification was performed using an AKTA Purifier UP900 system. The purification workflow included anion-exchange chromatography, cation-exchange chromatography, and gel filtration chromatography.

Anion-Exchange Chromatography

2 mL of venom supernatant was loaded onto a DEAE-Sepharose Fast Flow column (10×100 mm, 7 mL) pre-equilibrated with five column volumes of Tris-HCl buffer (pH 8.0, 10 mM). Gradient elution was performed over 25 column volumes using a linear gradient of NaCl solution (0-0.5 M) at a constant flow rate of 0.5 mL/min. Throughout the elution process, UV absorbance at 280 nm (A_{280}) was continuously monitored. Fractions corresponding to the chromatographic peaks were collected, desalted using an Amicon® Ultra-0.5 mL Centrifugal Filters (3 kDa, UFC5003, MilliporeSigma), and washed three times with ddH_2O, followed by determination of the cell proliferation Inhibition Rate (IR).

Cation-Exchange Chromatography

The fraction exhibiting the highest tumor cell inhibition rate from anion-exchange chromatography was concentrated using Amicon® Ultra-0.5 mL Centrifugal Filters (3 kDa, UFC5003, MilliporeSigma), washed three times with ddH_2O, and buffer-exchanged into 10 mM NaH_2PO_4 (pH 5.7) to prepare working samples. These samples were loaded onto an SP-Sepharose Fast Flow column (10×100 mm, 7 mL) pre-equilibrated with five column volumes of NaH_2PO_4 buffer (pH 5.7, 10 mM). Linear gradient elution was performed over 25 column volumes with NaCl solution (0-0.5 M) at a flow rate of 0.5 mL/min. UV absorbance at 280 nm (A_{280}) was continuously monitored throughout the separation. Fractions corresponding to the chromatographic peaks were collected, desalted using an Amicon® Ultra-0.5 mL Centrifugal Filters (3 kDa, UFC5003, MilliporeSigma), and washed three times with ddH_2O followed by determination of the cell proliferation IR.

Gel Filtration Chromatography

The fraction exhibiting the highest tumor cell inhibition rate from cation-exchange chromatography was concentrated using Amicon® Ultra-0.5 mL Centrifugal Filters (3 kDa, UFC5003, MilliporeSigma), washed three times with ddH_2O, and buffer-exchanged into ddH_2O to prepare working samples. These samples were loaded onto a Sephadex G-75 column (16 umn) 16 d onto a Sephadex G-75 column (16 reSigma), washed thrddH_2O. Isocratic elution was conducted using 25 column volumes of ddH_2O at a flow rate of 0.3 mL/min. Throughout the separation, UV absorbance at 280 nm (A_{280}) was monitored. The collected fractions were concentrated using Amicon® Ultra-0.5 mL centrifugal filter devices (3 kDa, UFC5003; MilliporeSigma), washed three times with ddH_2O, stored at -80°C, and labeled as 'FS-1' for subsequent analysis.

Detection Assay for Tumor Cell Proliferation IR

Logarithmically growing HeLa and Hep G2 cells were seeded in 96-well plates at 8,000 cells per well. Protein fractions corresponding to chromatographic peaks were tested at 20 µg/mL, with camptothecin (1 µM) as positive control and ddH_2O as

negative control. Following 48-hr incubation at 37°C in a 5% CO_2 humidified atmosphere, cellular viability was determined using an MTT assay kit (C0009S, Beyotime, China). Three independent experiments were performed with three measurements per experiment. Absorbance values were normalized against controls, assigning 100% viability to camptothecin-treated samples and 0% to ddH_2O controls. The formula for calculating IR is as follows:

$$IR\ (\%)=(OD\ negative\ control\ group - OD\ experimental\ group)/(OD\ negative\ control\ group - OD\ positive\ control\ group) \times 100\%$$

SDS-PAGE

Following the protocol provided by the SDS-PAGE kit （P0012AC, Beyotime, China), we selected a 12% separating gel and a 5% stacking gel. The gels were then stained with Coomassie Blue Staining Kit (P0017A, Beyotime, China) for visualization.

FS-1 Inhibition of HeLa and Hep G2 Cell Proliferation

HeLa and Hep G2 cells in the exponential growth phase were seeded in 96-well plates at 8,000 cells per well and cultured at 37°C in a 5% CO_2 incubator. The experimental groups were treated with whole snake venom and FS-1 fraction, using camptothecin as the positive control and ddH_2O as the negative control, with protein concentration gradients set at 128, 64, 32, 16, 8, 4, 2, 1, and 0.5 μg/mL. Cells were harvested at 12, 24, 48, 72, and 96 hr, washed with PBS, and subjected to MTT assay kit (C0009S, Beyotime, China) for viability assessment. The experiment was repeated three times with triplicate absorbance measurements. Cell viability was normalized to the positive control (100%) and negative control (0%) to calculate IR. The IR values obtained at each concentration across 12-96 hr were then subjected to regression analysis (95% confidence interval) to determine the half-maximal Inhibitory Concentration (IC_{50}), with the 48-hr data used to plot IR versus IC_{50} curves.

FS-1 Induced Phosphatidylserine (PS) Externalization in Tumor Cells

The externalization of PS on the plasma membrane was assessed using the Annexin V-FITC/PI dual-staining apoptosis detection kit (BB-4101, Bestbio, China) according to the manufacturer's instructions. Log-phase HeLa and Hep G2 cells were seeded in 96-well plates at a density of 2×10^4 cells per well and cultured for 24 hr. A blank control and an FS-1-treated experimental group were established. In the experimental group, FS-1 was added at final concentrations of 10 μg/mL for HeLa cells and 15 μg/mL for Hep G2 cells. After 6 hr of incubation, the culture was terminated, and the cells were harvested by digestion with 0.25% trypsin, washed with PBS, and collected by centrifugation. The cell pellets were resuspended in 400 μL of Annexin V binding buffer, followed by the addition of 5 μL of Annexin V-FITC. The samples were incubated in the dark at 4°C for 15 min. Subsequently, 10 μL of Propidium Iodide (PI) staining solution was added, gently mixed, and incubated in the dark at 4°C for an additional 4 min. Immediately observe the cells under a fluorescence microscope and record them.

Mitochondrial Permeability Transition Pore (MPTP) experiment

Log-phase HeLa and Hep G2 cells were seeded in 96-well plates and incubated at 37°C in a 5% CO_2 atmosphere for 24 hr. The culture medium was then replaced with fresh medium containing FS-1 at final concentrations of 10 μg/mL for HeLa cells and 15 μg/mL for Hep G2 cells. After 36 hr of treatment, the culture medium was removed, and the cells were washed twice with PBS. MPTP opening was assessed following the protocol of the Mitochondrial Permeability Transition Pore experiment Kit (C2009S, Beyotime, China).

DNA Damage experiment

Log-phase HeLa and Hep G2 cells were cultured in T25 flasks for 24 hr at 37°C with 5% CO_2. FS-1 was then added at final concentrations of 10 μg/mL for HeLa cells and 15 μg/mL for Hep G2 cells. After 48 hr of incubation, cells were collected, and DNA was extracted for agarose gel electrophoresis to assess fragmentation. DNA extraction followed the protocol provided in the Apoptosis DNA Ladder Extraction Kit with Spin Column (C0008, Beyotime, China). The control group was cultured under identical conditions without FS-1 treatment.

Molecular Mechanism of FS-1-Induced Apoptosis in Tumor Cells

HeLa and Hep G2 cells in the logarithmic growth phase were cultured in T25 flasks at 37°C with 5% CO_2 for 24 hr. A blank control and an FS-1-treated experimental group were established. In the experimental group, FS-1 was added to the culture medium at final concentrations of 10 μg/mL for HeLa cells and 15 μg/mL for Hep G2 cells. Cells were incubated under these conditions, and various molecular markers of apoptosis were analyzed at specific time points. The concentration of BAD protein was measured at 12 hr; Cyt C, BAX, Bcl-2, and Bcl-xl at 24 hr; caspase-8 and caspase-9 activities at 36 hr; and caspase-3 and caspase-6 activities, along with Western blot analysis, at 48 hr.

Cyt C Concentration Determination

Mitochondria were isolated from the cells, and Cyt C concentrations in both the cytosol and mitochondria were measured in the experimental and control groups. Mitochondrial isolation was performed using the Mitochondrial Isolation Kit (C3601, Beyotime, China), and Cyt C concentration was determined using the Cyt C ELISA Kit (ml106292, mlbio, China). Cells were lysed using a glass homogenizer, and the supernatant obtained after mitochondrial isolation was used to measure cytosolic Cyt C concentration. Mitochondria were lysed with

mitochondrial lysis buffer to determine the mitochondrial Cyt C concentration. The Optical Density (OD) was measured at 450 nm.

Bcl-2 Family Protein Concentration Determination

The concentrations of Bcl-2, Bcl-xl, BAD, and BAX proteins were measured using an ELISA kit (mlbio, China) according to the manufacturer's instructions. Cells were lysed using a glass homogenizer, centrifuged at 1,000 g for 10 min, and the supernatant was collected. The protein concentration was determined using the BCA method, and OD was measured at 450 nm.

Caspase Family Protease Activity Experiment

The activities of caspase-3, caspase-6, caspase-8, and caspase-9 were determined using a caspase activity experiment kit (Beyotime, China) following the manufacturer's protocol. The experiment detects the release of *pNA* from specific caspase substrates. Cell lysates were incubated with *Ac-DEVD-pNA* at 37°C for 1 hr, and absorbance was measured at 405 nm. One unit (U) is the amount of enzyme that will cleave 1 nmol of the colorimetric substrate *Ac-DEVD-pNA* per hour at 37°C under saturated substrate concentrations.[13] The calculation formula is as follows:

$$\text{Enzyme activity (U)} = \text{Amount of pNA produced (nmol)} / \text{Reaction time (hour)}$$

Western Blot Analysis

For the experimental group, cytosolic fractions were collected at 24 hr for Apoptosis-Inducing Factor (AIF), Bcl-2, and Bcl-xl analysis, and at 36 hr for caspase-3 and caspase-6 analysis. Protein concentrations were determined using the BCA Protein experiment Kit (P0010S, Beyotime, China) and normalized to equal concentrations. Samples were mixed with SDS-PAGE loading buffer (P0963-2 mL, Beyotime, China) and boiled for 5 min for denaturation. After cooling, 20 µL of each sample was loaded onto an SDS-PAGE gel, using a 12% resolving gel and a 5% stacking gel. Electrophoresis was performed at 80 V for 30 min, followed by 120 V for 100 min. Proteins were transferred onto a PVDF membrane (FFP19, Beyotime, China) using a wet transfer system at 350 mA for 45 min. The membrane was blocked, incubated with primary and secondary antibodies (both from Beyotime, China), and visualized using the ECL Chemiluminescence Kit (P0018S, Beyotime, China).

Statistical Analysis

Statistical analysis was performed using SPSS software (version 27.0). Data normality was verified by Shapiro-Wilk test. For comparisons between two groups, unpaired Student's *t*-test was applied when data followed a normal distribution; otherwise, the Mann-Whitney U test was used. Each molecular marker (e.g., BAD, BAX, Bcl-2, Bcl-xl, Cyt C, Caspase-3, Caspase-6, Caspase-8, Caspase-9) was analyzed as an independent hypothesis test. Data are presented as mean±SD of three independent biological replicates (each with three technical replicates). Statistical significance was set at $p<0.05$.

The Half-Maximal Inhibitory Concentration (IC_{50}) values were determined using GraphPad Prism 9.0 (GraphPad Software, San Diego, CA). Dose-response data were fitted to a four-Parameter Logistic (4PL) nonlinear regression model with the following equation:

$$Y=(\text{Bottom} \times \text{lgIC50}-X)\times\text{HillSlope} + \text{Top}) / (1 + \text{lgIC50} -X)\times\text{HillSlope})$$

Where "Y" is the inhibition rate (%), "X" is the logarithm of FS-1 concentration (µg/mL), "Top" is the maximum inhibition plateau (constrained to 100%), "Bottom" is the minimum inhibition plateau (constrained to 0%), and "HillSlope" is the curve steepness parameter. IC_{50} values and their 95% confidence intervals were derived from the fitted curves. The model goodness-of-fit was verified by $R^2>0.97$ for all analyses.

RESULTS

Anion-Exchange Chromatography

Five distinct peaks were obtained from the DEAE-Sepharose Fast Flow chromatography of the *Gloydius brevicaudus* venom reserve supernatant, designated as X, A, B, C, and D (Figure 1A). Among them, peak X represented the flow-through fraction (proteins not bound to DEAE-Sepharose). The collected protein fractions were then concentrated and desalted for further *in vitro* tumor cell proliferation inhibition assays (Figure 1).

The IR for each fraction were as follows: Peak X protein exhibited an IR of 3.55±0.026% on HeLa cells and 14.17±0.019% on Hep G2 cells. Peak A protein exhibited an IR of 4.43±0.025% on HeLa cells and 8.91±0.025% on Hep G2 cells. Peak B protein showed the highest inhibition, with an IR of 93.85±0.015% on HeLa cells ($p<0.01$ vs all other peaks) and 95.39±0.08% on Hep G2 cells ($p<0.001$ vs all other peaks). Peak C protein had an IR of 7.59±0.054% on HeLa cells and 11.7±0.025% on Hep G2 cells, while peak D protein demonstrated an IR of 4.2±0.017% on HeLa cells and 13.1±0.014% on Hep G2 cells (Figure 1D).

These results indicate that peak B protein exhibited the strongest inhibitory effect on tumor cell proliferation. Consequently, the protein from peak B was selected for further experiments.

Cation-Exchange Chromatography

The protein solution from peak B, obtained through anion-exchange chromatography, was desalted, and the buffer (pH 5.4, 0.01 M NaH_2PO_4) was replaced using ultrafiltration. A total of 2 mL of this protein solution was then injected into a cation-exchange chromatography column (SP-Sepharose Fast Flow) for further purification. This process yielded three distinct

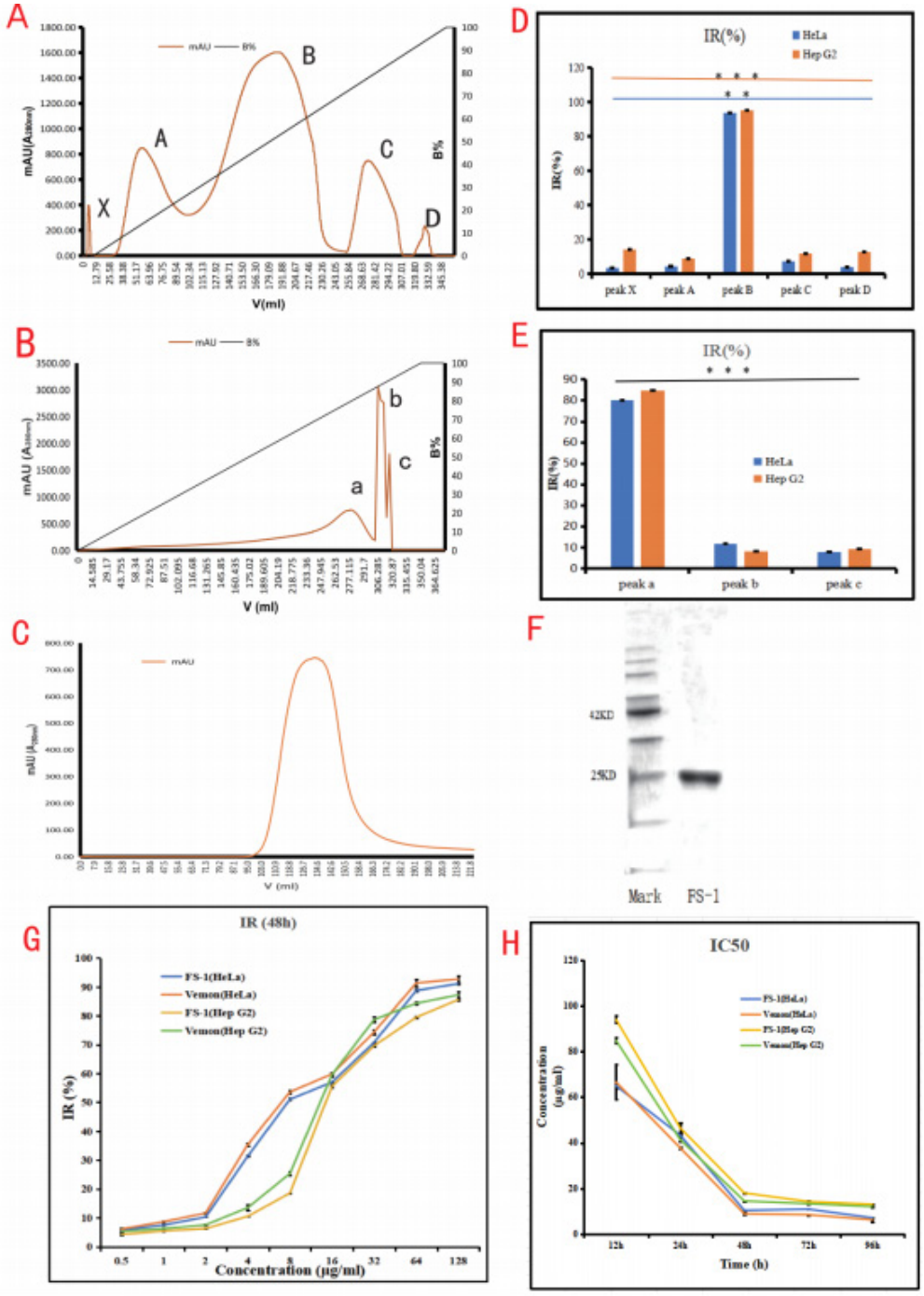

Figure 1: Isolation of Tumor-Inhibitory Components from *Gloydius brevicaudus* Venom. Note: A. Anion exchange chromatography; B. Cation exchange chromatography; C. Gel filtration chromatography; D. Inhibition of tumor cell proliferation activity by five UV-absorption peak proteins after anion exchange chromatography; E. Inhibition of tumor cell proliferation activity by three UV-absorption peak proteins after cation exchange chromatography; F. SDS-PAGE electrophoresis of the absorption peaks following gel filtration chromatography; G. Dose response of FS-1 to inhibit proliferation of Hela and Hep G2 cell lines, H. Time-response of FS-1 to inhibit proliferation of Hela and Hep G2 cell lines. Values are Mean ± SD of three biological replicates (each with three technical replicates).

UV-absorption peaks (A_{280} nm), designated as peaks a, b, and c (Figure 1B). The proteins corresponding to each peak were subsequently concentrated and desalted for *in vitro* tumor cell proliferation inhibition assays.

The IR of the purified proteins were as follows: Peak a protein exhibited an IR of 80.28±0.043% on HeLa cells (p<0.001 vs all other peaks) and 84.73±0.052% on Hep G2 cells (p<0.001 vs all other peaks). Peak b protein showed a significantly lower IR, with 11.84±0.036% on HeLa cells and 8.22±0.037% on Hep G2 cells. Similarly, peak c protein displayed minimal inhibition, with an IR of 7.8±0.043% on HeLa cells and 9.29±0.074% on Hep G2 cells (Figure 1E).

These findings indicate that peak a protein exhibited the strongest tumor cell proliferation inhibitory effect. Therefore, protein from peak a was selected for further experiments.

Gel Chromatography

The protein from peak a, collected through cation-exchange chromatography, was subjected to gel filtration on Sephadex G-75, yielding a single peak (Figure 1C). This peak corresponded to a band with a relative molecular mass of approximately 25 kDa, as determined by SDS-PAGE (Figure 1F). This protein was named FS-1 and was subsequently investigated in tumor inhibition proliferation experiments.

FS-1 Inhibition of HeLa and Hep G2 Cell Proliferation

FS-1 exhibited concentration-dependent inhibitory effects on the proliferation of both HeLa and Hep G2 cell lines, characterized by a sigmoidal dose-response curve. At concentrations of 4-64 μg/mL for HeLa cells and 8-128 μg/mL for Hep G2 cells, the inhibition rate increased linearly with concentration (Figure 1G).

FS-1 also demonstrated time-dependent inhibition in both cell lines. The IC_{50} decreased with prolonged exposure time (12-96 hr), with 48 hr identified as the optimal incubation period. Notably, comparable inhibition was achieved at lower concentrations with longer exposure (≥48 hr) or higher concentrations with shorter exposure. Beyond 48 hr, the rate of IC_{50} reduction slowed, and values plateaued at higher concentrations (Figure 1H). Thus, 48 hr was selected as the reference time point for subsequent studies.

FS-1 and*Gloydius brevicaudus* venom exhibited similar trends in IC_{50} values against HeLa and Hep G2 cells. The IC_{50} values were calculated using a nonlinear regression model (four-parameter logistic curve, 4PL) with a goodness-of-fit R^2>0.97 (Table 2).

FS-1 Induced Tumor Cell Membrane PS Externalization experiment

After treating HeLa and Hep G2 cells with FS-1 for 6 hr, dual staining with annexin V-FITC and PI revealed distinct apple-green fluorescence on the cell membranes of both cell lines under a fluorescence microscope, with no red fluorescence observed. In contrast, control cells, which underwent the same staining procedure, showed no fluorescence (Figure 2).

Bcl-2 Family Protein Concentration Determination

After 12 hr of FS-1 treatment, BAD expression in HeLa cells increased significantly from 897.51±11.790 ng/mg in the control group to 1015.15±23.974 ng/mg in the experimental group (p=0.005). Similarly, in Hep G2 cells, BAD expression increased from 966.34±2.555 ng/mg to 1058.33±4.390 ng/mg (p=0.00004) (Table 1).

After 24 hr of FS-1 treatment, BAX expression in HeLa cells increased significantly from 2.24±0.002 ng/mg in the control group to 2.51±0.037 ng/mg in the experimental group (p=0.006).

Table 1: Detection of Apoptosis-Related Factors in HeLa and Hep G2 Cells.

		Cyt C ng/mL		BAD ng/mL	BAX ng/mL	Bcl-2 ng/mL	Bcl-xl ng/mL	Caspase 3 U	Caspase 6 U	Caspase 8 U	Caspase 9 U
		Cytoplasm	Mitochondrion								
Hela	Experimental	16.83±0.685^b	13.23±0.181^b	1015.15±23.974^b	2.51±0.037^b	52.80±0.166^c	37.50±0.236^c	3.69±0.071^b	3.59±0.035^c	4.01±0.039^a	3.11±0.025^b
	Control	12.24±0.316	17.60±0.674	897.51±11.790	2.24±0.002	54.73±0.224	41.46±0.217	3.39±0.059	3.03±0.008	3.91±0.014	2.94±0.007
Hep G2	Experimental	17.61±1.208^a	12.23±0.344^a	1058.33±4.390^c	2.28±0.007^a	48.19±0.504^c	36.21±1.085^b	3.79±0.023^c	3.80±0.022^c	4.32±0.104^a	3.28±0.035^b
	Control	14.51±0.614	16.83±1.833	966.34±2.555	2.20±0.020	62.13±1.019	47.43±0.408	3.18±0.052	3.25±0.022	4.03±0.039	3.08±0.037

Not: Values are mean±SD ng/mL of three biological replicates (each with three technical replicates); a: p<0.05; b: p<0.01; c: p<0.001.

Table 2: IC_{50} values of FS-1 and snake venom at different time points.

		Time(h)	12			24			48			72			96		
			IC_{50} (μg/mL)	95% CI	R^2	IC_{50} (μg/mL)	95% CI	R^2	IC_{50} (μg/mL)	95%CI	R^2	IC_{50} (μg/mL)	95% CI	R^2	IC_{50} (μg/mL)	95% CI	R^2
Hela	FS-1	1	66.11	56.30 - 79.19	0.99	43.92	34.05-58.86	0.98	10.43	8.41-12.97	0.99	10.91	9.25 - 12.88	0.99	7.19	5.85 - 8.87	0.99
		2	63.56	55.39 - 73.93	0.99	43.26	33.95 -57.01	0.98	10.36	8.27 -13.00	0.98	10.92	9.27 - 12.88	0.99	7.05	5.71 - 8.74	0.99
		3	65.1	54.42 -79.83	0.99	42.71	33.43 - 56.42	0.98	10.28	8.18 -12.94	0.98	10.83	9.15 - 12.83	0.99	7.01	5.70 - 8.64	0.99
		Average	64.92			43.30			10.36			10.89			7.08		
		STD V	1.28			0.61			0.08			0.05			0.09		
	Snak venom	1	75.14	61.45 - 95.15	0.99	38.18	31.84 - 46.44	0.99	8.79	6.94 - 11.16	0.98	8.6	6.96 - 10.59	0.99	7.19	5.85 - 8.87	0.99
		2	63.96	55.63 - 74.59	0.99	37.69	31.14 - 46.41	0.99	9.14	7.31 - 11.46	0.98	8.44	6.74 - 10.54	0.98	5.59	4.69 - 6.67	0.99
		3	60.5	52.41 - 70.85	0.99	37.34	30.72 - 46.22	0.99	8.74	6.94 - 11.01	0.98	8.33	6.57 - 10.53	0.98	5.92	4.97 - 7.05	0.99
		Average	66.53			37.74			8.89			8.46			6.23		
		STD V	7.65			0.42			0.22			0.14			0.84		
Hep G2	FS-1	1	93.92	75.57 - 122.0	0.99	47.32	38.99 - 58.72	0.99	18.14	14.08- 23.59	0.98	14.44	12.35-16.91	0.99	13.18	11.70-14.87	0.99
		2	92.21	73.34 - 121.8	0.98	45.56	37.44 - 56.68	0.99	17.95	14.13-22.99	0.98	13.98	12.02-16.29	0.99	13.06	11.61-14.71	0.99
		3	94.85	76.17 - 123.6	0.99	46.60	38.87 - 56.95	0.99	17.81	13.77-23.26	0.97	14.24	12.19-16.68	0.99	12.8	11.41-14.38	0.99
		Average	93.66			46.49			17.97			14.22			13.01		
		STD V	1.34			0.88			0.17			0.23			0.19		
	Snak venom	1	86.41	71.38 - 108.0	0.99	43.86	37.11 - 52.65	0.99	13.9	11.37-17.03	0.98	13.33	11.39-15.62	0.99	11.90	10.61-13.35	0.99
		2	83.16	65.81 - 110.3	0.98	40.42	33.49 - 49.69	0.99	14.66	11.81- 18.27	0.98	13.50	11.56-15.80	0.99	11.88	10.63-13.28	0.99
		3	84.79	70.79 - 104.4	0.99	39.79	34.17 - 46.88	0.99	14.26	11.18- 18.31	0.98	13.09	11.26-15.24	0.99	12.27	10.95-13.77	0.99
		Average	84.79			41.36			14.46			13.31			12.02		
		STD V	1.63			2.19			0.28			0.21			0.22		

Similarly, in Hep G2 cells, BAX expression increased from 2.20±0.020 ng/mg to 2.28±0.007 ng/mg (p=0.0013). Bcl-2 expression in HeLa cells reduced significantly from 54.73±0.224 ng/mg in the control group to 52.80±0.166 ng/mg in the experimental group (p=0.0004). Similarly, in Hep G2 cells, Bcl-2 expression reduced from 62.13±1.019 ng/mg to 48.19±0.504 ng/mg (p=0.0003). Bcl-xl expression in HeLa cells reduced significantly from 41.46±0.217 ng/mg in the control group to 37.50±0.236 ng/mg in the experimental group (p=0.00003). Similarly, in Hep G2 cells, Bcl-xl expression reduced from 47.43±0.408 ng/mg to 36.21±1.085 ng/mg (p=0.0011) (Table 1).

Mitochondrial Permeability Transition Pore (MPTP) experiment

Cells from both the FS-1-treated experimental group and the control group were collected separately for analysis. Following the addition of the calcein AM fluorescent probe, both groups exhibited strong green fluorescence. Upon adding $CoCl_2$, the experimental group showed a complete disappearance of the green fluorescence, whereas in the control group, the fluorescence was only partially quenched, with weak green fluorescence remaining in the cells. This observation suggests that in the experimental group, the mitochondrial MPTP was opened, allowing Co^{2+} to enter the mitochondria and quench the fluorescence. In contrast, the MPTP remained closed in the control group, preventing the entry of Co^{2+} and preserving mitochondrial green fluorescence, while the cytoplasmic fluorescence was quenched.[14]

When ionomycin, a calcium ion carrier, was added to the control group, the green fluorescence was completely quenched as Ca^{2+} entered both the cells and mitochondria. This influx of Ca^{2+} caused mitochondrial Ca^{2+} overload, triggering the opening of the MPTP, which allowed Co^{2+} to enter the mitochondria and quench the green fluorescence. These findings indicate that FS-1 induces the opening of the mitochondrial MPTP (Figure 3).

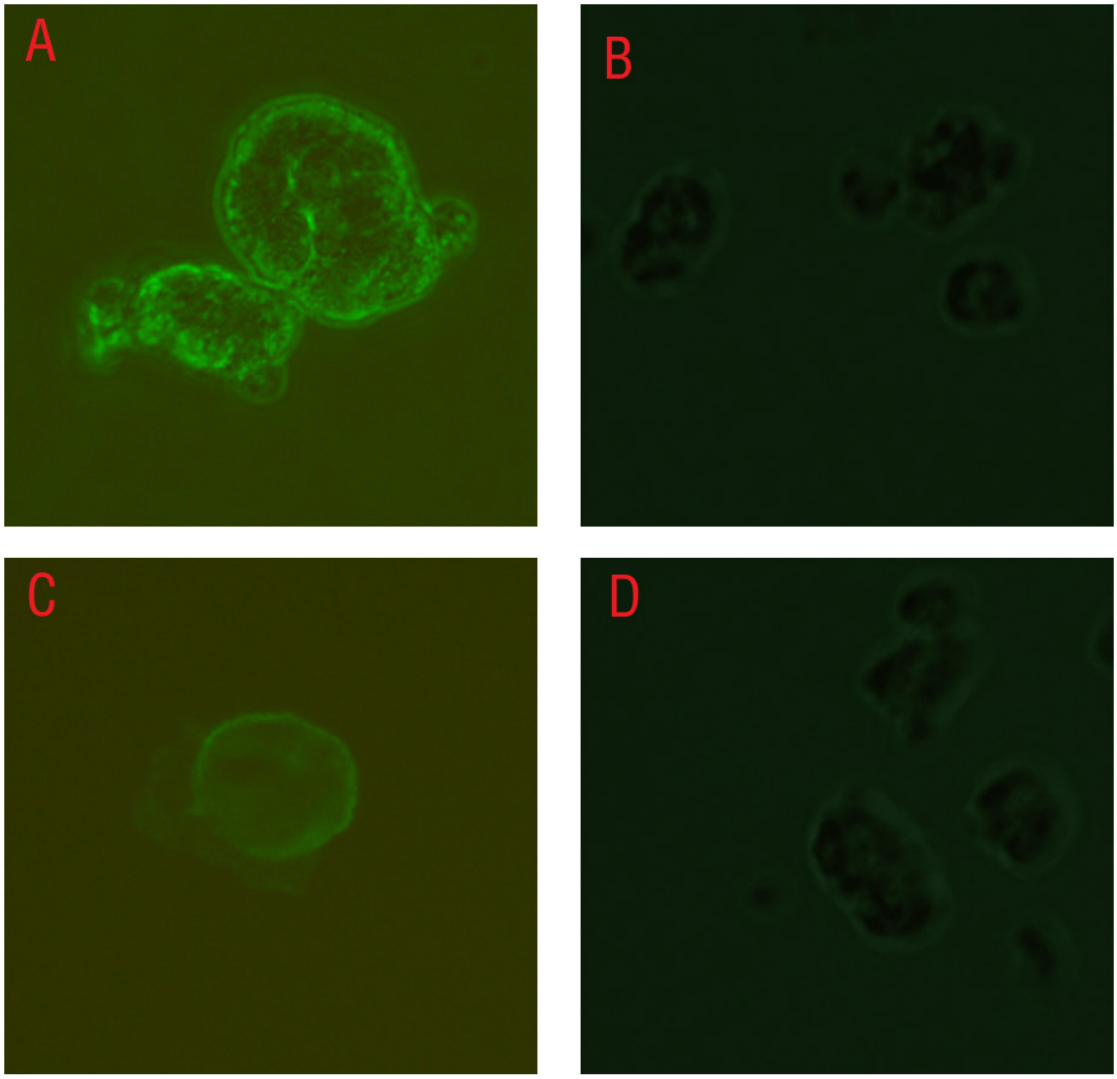

Figure 2: FS-1 Induced Tumor Cell Membrane Phosphatidylserine (PS) Externalization Assay (magnification 20x20). Note: A. Hela cells experimental group; B. Hela cells control group; C. Hep G2 cells experimental group; D. Hep G2 cells control group.

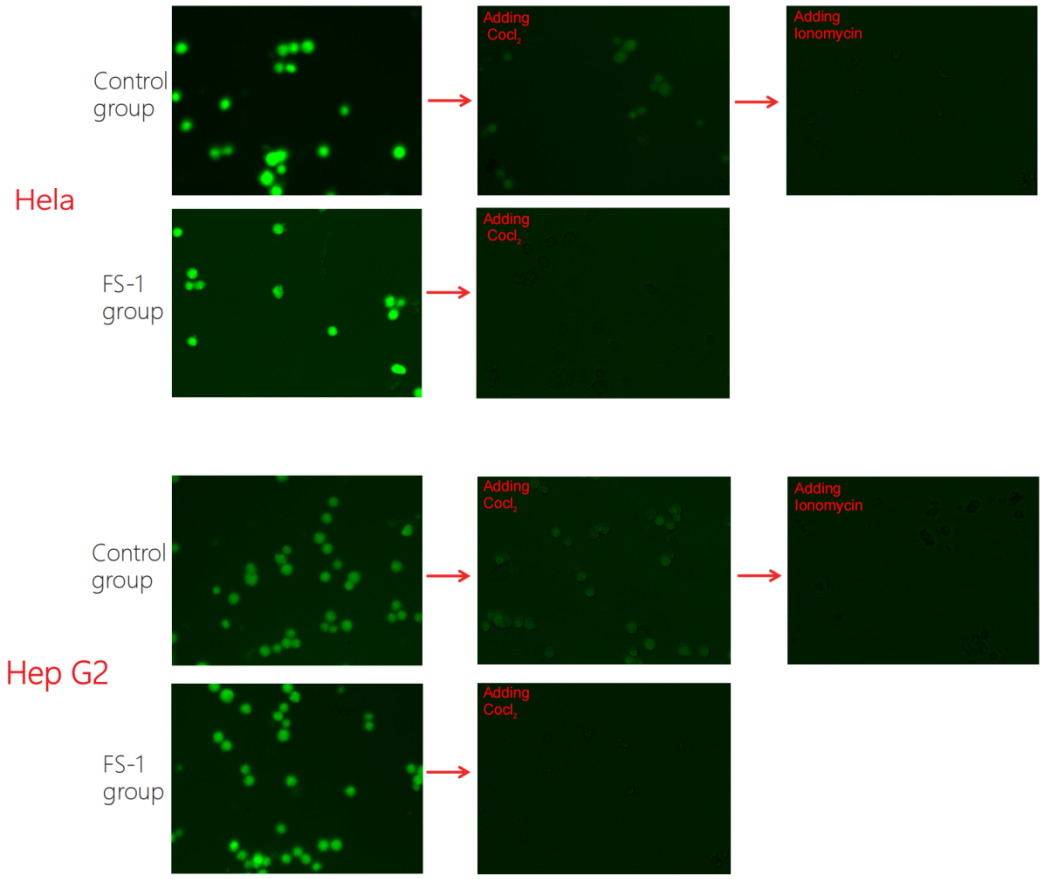

Figure 3: Mitochondrial Permeability Transition Pore (MPTP) Assay (magnification 10x20).

Cyt C Concentration

Following 24 hr of FS-1 treatment, mitochondrial Cyt C levels in HeLa cells significantly decreased from 17.60±0.674 ng/mg to 13.23±0.181 ng/mg (p=0.002). Conversely, cytosolic Cyt C levels increased from 12.24±0.316 ng/mg to 16.83±0.685 ng/mg (p=0.005). Similarly, in Hep G2 cells, mitochondrial Cyt C levels significantly decreased from 16.83±1.833 ng/mg to 12.23±0.344 ng/mg (p=0.029), while cytosolic levels increased from 14.51±0.614 ng/mg to 17.61±1.208 ng/mg (p=0.045). These changes indicate FS-1-induced Cyt C translocation from mitochondria to cytosol (Table 1).

Caspase Family Protease Activity Experiment

After 48 hr of FS-1 treatment, caspase-3 activity in HeLa cells increased significantly from 3.39±0.059 U in the control group to 3.69±0.071 U in the experimental group (p=0.005). Similarly, in Hep G2 cells, caspase-3 activity increased from 3.18±0.052 U to 3.79±0.023 U (p=0.0006). Caspase-6 activity in HeLa cells increased significantly from 3.03±0.008 U in the control group to 3.59±0.035 U in the experimental group (p=0.0008). Similarly, in Hep G2 cells, caspase-6 activity increased from 3.25±0.022 U to 3.80±0.022 U (p=0.000006) (Table 1).

After 36 hr of FS-1 treatment, caspase-8 activity in HeLa cells increased significantly from 3.91±0.014 U in the control group to 4.01±0.039 U in the experimental group (p=0.029). Similarly, in Hep G2 cells, caspase-8 activity increased from 4.03±0.039 U to 4.32±0.104 U (p=0.028). Caspase-9 activity in HeLa cells increased significantly from 2.94±0.007 U in the control group to 3.11±0.025 U in the experimental group (p=0.005). Similarly, in Hep G2 cells, caspase-9 activity increased from 3.08±0.037 U to 3.28±0.035 U (p=0.003) (Table 2).

Western Blot Analysis

To further elucidate the molecular mechanisms underlying cell apoptosis, Western blot analysis was performed to examine the expression levels of caspase-3, caspase-6, Bcl-2, Bcl-xl, and AIF. The results demonstrated downregulation of anti-apoptotic proteins Bcl-2 and Bcl-xl, along with upregulated expression of caspase-3 and caspase-6 proteins. These findings were consistent with the decreased concentrations detected in the Bcl-2 protein family and increased activity observed in the caspase protein family. Additionally, elevated expression of AIF protein was detected (Figure 4).

DNA Damage experiment

HeLa and Hep G2 cells were treated with FS-1 for 48 hr, after which DNA was extracted and subjected to agarose gel electrophoresis. DNA fragments smaller than 100 bp were observed in the FS-1-treated groups, while no such fragments were detected in the

control group, indicating that FS-1 exposure led to DNA damage in the cells (Figure 5).

DISCUSSION

In this study, a tumor apoptosis-inducing protein, FS-1, was isolated from *Gloydius brevicaudus* venom. SDS-PAGE analysis revealed a band at 25 kDa, which is comparable to the molecular weight of antitumor proteins reported in *Deinagkistrodus acutus* venom.[15]

Tumor cell apoptosis involves a series of morphological changes triggered by apoptotic factors, with the first alterations occurring at the cell membrane. Upon exposure to apoptotic signals, specific receptors on the cell membrane mediate the externalization of

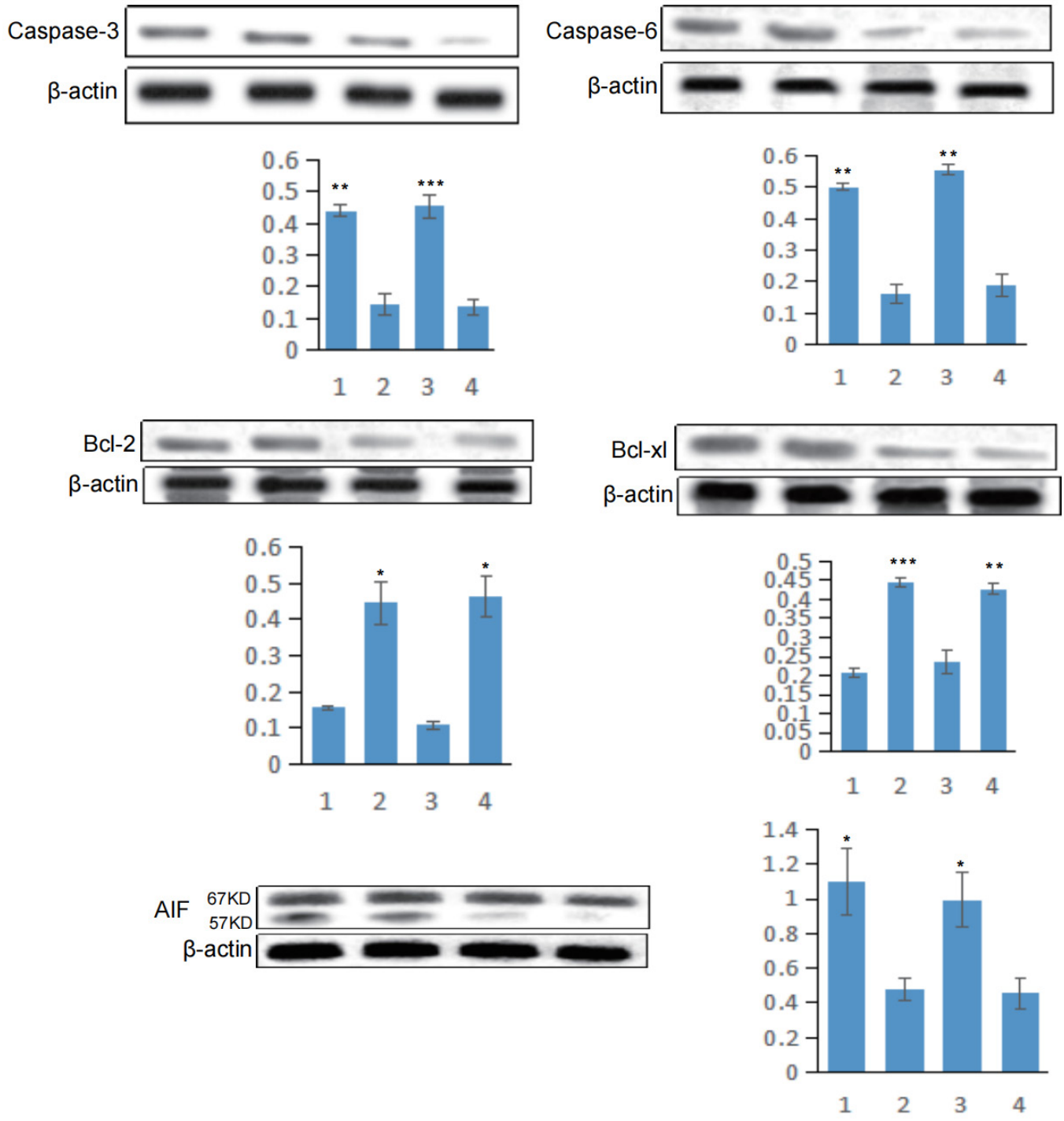

Figure 4: Western Blot Analysis. Note: 1. Hela experimental group; 2. Hela control group; 3. Hep G2 experimental group; 4. Hep G2 control group. Values are Mean ± SD of three biological replicates (each with three technical replicates).

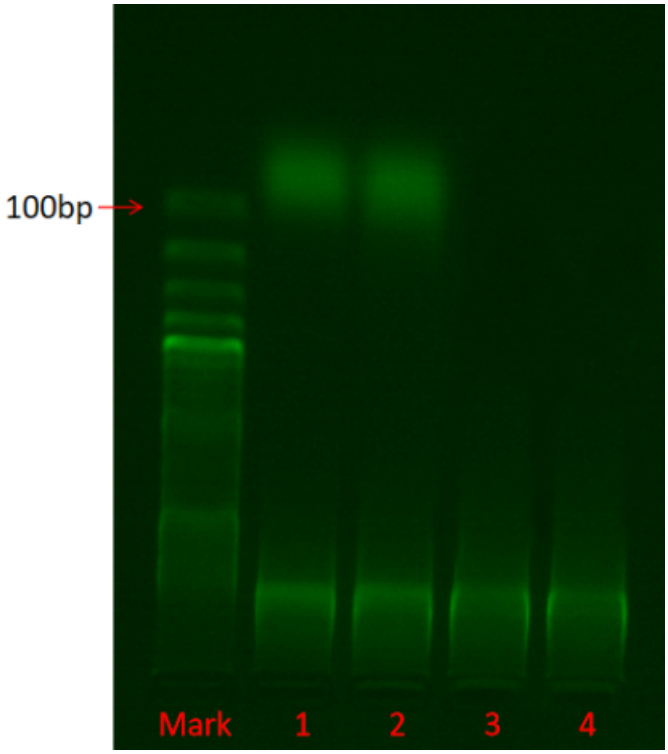

Figure 5: Agarose Gel Electrophoresis of DNA. Note: 1. Hela cell experimental group; 2. Hep G2 cell experimental group; 3. Hela cell control group; 4. Hep G2 cell control group.

PS from the inner leaflet to the outer leaflet, whereas in normal cells, PS is predominantly confined to the inner leaflet. When FITC-labeled annexin V binds to the exposed PS, it forms a distinct green fluorescent layer on the outer membrane, which is clearly visible under a fluorescence microscope.[16]

In viable, non-apoptotic cells, annexin V-FITC does not bind to PS because PS remains confined to the inner leaflet of the plasma membrane, resulting in no green fluorescence. In contrast, when membrane integrity is compromised, annexin V-FITC can penetrate the cell and produce a fluorescent signal. To distinguish necrotic cells from apoptotic ones, PI is used in combination with annexin V-FITC. PI selectively enters cells with damaged membranes, binds to nucleic acids, and emits red fluorescence, whereas intact cells exclude PI and do not display red fluorescence. This dual staining method enables a clear differentiation between apoptotic and necrotic cells.[17]

Dual staining with annexin V-FITC and PI revealed distinct apple-green fluorescence on the plasma membranes of both HeLa and Hep G2 cells 6 hr after FS-1 treatment, with no red fluorescence observed (control cells showed neither fluorescence). This pattern suggests early apoptotic signaling through PS externalization. While these observations implicate membrane-mediated initiation of apoptosis, the precise mechanism underlying PS translocation merits further investigation.[18]

BAD and BAX are pro-apoptotic members of the Bcl-2 family. After apoptotic signals are transmitted intracellularly, the expression of BAD is induced. The increase in BAD may also result from its phosphorylation upon receiving these signals, which leads to its dissociation from the Bcl-2 and Bcl-xL aggregates. In normal cells, BAD binds to the anti-apoptotic proteins Bcl-2 or Bcl-xL, forming complexes that inhibit apoptosis.[19,20] Upon receiving apoptotic signals, BAD becomes phosphorylated, leading to its dissociation from Bcl-2 or Bcl-xL. Under non-apoptotic conditions, BAX is primarily cytosolic and inactive; however, following apoptotic stimuli, BAX undergoes a conformational change and translocates to the mitochondrial outer membrane,[21] where it associates with phosphorylated BAD to increase mitochondrial membrane permeability.[22-25] Additionally, BAX interacts with other Bcl-2 family members, such as BAD and Bak, to further enhance mitochondrial membrane permeability.[26]

In contrast, Bcl-2 and Bcl-xL are anti-apoptotic proteins within the Bcl-2 family, and their reduced expression facilitates apoptosis in HeLa and Hep G2 cells. Bcl-2 is localized to the outer mitochondrial membrane and primarily functions to inhibit MPTP opening, thereby preventing the release of Cyt C.[27,28] A dynamic balance between Bcl-2 and BAX is essential for regulating cell survival or apoptosis. Bcl-2 inhibits BAX activation and the opening of the MPTP, thereby preventing the initiation of apoptotic signaling pathways.[29,30] The anti-apoptotic function of Bcl-xL is achieved through three mechanisms: (1) Maintaining mitochondrial membrane integrity by binding to the mitochondrial membrane and preventing its rupture along with the release of Cyt C; (2) Inhibiting caspase family protease activity through direct interactions;[31,32] and (3) Regulating intracellular

calcium concentrations to preserve cellular calcium homeostasis, which is critical for controlling apoptosis.[33,34]

The MPTP opening assay indicates that pro-apoptotic proteins induce the opening of the MPTP. Mitochondria, as double-membrane organelles, play a crucial role in protecting cellular components and maintaining membrane potential, which is essential for the proper function of the electron transport chain and oxidative phosphorylation. The integrity of the mitochondrial membrane is pivotal in regulating apoptosis. The MPTP, also known as the Mitochondrial Megachannel (MMC), is a non-selective channel formed by the inner and outer mitochondrial membranes. During apoptosis, the opening of the MPTP causes significant changes in mitochondrial permeability, which leads to the release of pro-apoptotic factors (such as Cyt C) into the cytoplasm, the collapse of mitochondrial membrane potential, disruption of the electron transport chain, and a failure in oxidative phosphorylation, all of which contribute to the induction of cell death.[35]

Subsequent Bcl-2 family dynamics revealed increased BAD/BAX and decreased Bcl-2/Bcl-xl expression at 12-24 hr. These shifts coincided temporally with mitochondrial MPTP opening and Cyt C redistribution-findings consistent with established models where pro-apoptotic Bcl-2 members promote mitochondrial permeability.[36] The concomitant reduction in anti-apoptotic proteins Bcl-2/Bcl-xl (known regulators of MPTP and Cyt C release) further supports mitochondrial involvement in FS-1-induced apoptosis.[37]

Caspase-3 and caspase-6 are key executioners in the apoptotic cascade, while caspase-8 and caspase-9 serve as crucial initiators of apoptotic signaling.[38] Activation of caspase-3 occurs via two primary pathways: the intrinsic and extrinsic pathways.[39,40] The intrinsic pathway is primarily driven by the release of Cyt C from the mitochondria, which binds to Apoptotic protease activating factor-1 (Apaf-1), forming an apoptosome that activates caspase-9. Activated caspase-9 subsequently activates caspase-3, which in turn activates caspase-6 to execute apoptosis.[41-43] The extrinsic pathway is initiated by extracellular stimuli that activate death receptors, triggering a cascade of protein interactions that ultimately activate caspase-8, which can then activate caspase-3 and induce apoptosis.[44] Caspase-8 may also indirectly activate caspase-6, enhancing the progression of apoptosis.[45,46] Once activated, caspase-3 triggers nuclear DNA fragmentation, degradation of structural proteins, and cytoskeletal disintegration, leading to the characteristic morphological and biochemical changes of apoptosis.[47,48] Caspase-3 and caspase-6 cooperate synergistically, with caspase-3 directly or indirectly activating caspase-6, enhancing the apoptotic response. Additionally, caspase-3 can inactivate caspase-6 inhibitors such as X-linked Inhibitor of Apoptosis Protein (XIAP), further promoting caspase-6 activity.[49-51]

In this study, we observed that caspase activation followed a sequential pattern: caspase-9 elevation at 36 hr aligned with Cyt C release (intrinsic pathway indicator), while concurrent caspase-8 enhancement may suggest extrinsic pathway contribution. Subsequent caspase-3/6 activation at 48 hr preceded DNA fragmentation-consistent with their roles as executioner caspases. The synergistic caspase-3/6 activity observed positions these proteases as terminal effectors in FS-1-induced apoptosis.

Notably, DNA fragmentation yielded atypically small fragments (<100 bp) rather than classical 180-200 bp ladders.[52] This pattern aligns with reports linking AIF to chromatin condensation and 50 bp fragmentation,[53-55] though cytoplasmic AIF localization in our study leaves nuclear translocation unconfirmed.[56,57]

This study provides preliminary characterization of an apoptosis-inducing protein component isolated from *Gloydius brevicaudus* venom, exploring its pro-apoptotic mechanisms. Our observations revealed a temporal profile of apoptotic events: PS externalization (6 hr), Bcl-2 dysregulation (12-24 hr), caspase activation (36-48 hr), and DNA damage (48 hr). While this sequence aligns with mitochondrial-caspase signaling, whether apoptosis induction is primarily reliant on this pathway warrants further validation and investigation.

There is insufficient consideration of alternative mechanisms for the observed effects, such as general cytotoxicity or off-target effects unrelated to apoptosis.

CONCLUSION

The protein FS-1, isolated from*Gloydius brevicaudus* venom, demonstrated antiproliferative and pro-apoptotic effects in HeLa and Hep G2 cells. Experimental observations revealed a sequential apoptotic cascade: PS externalization within 6 hr indicated apoptotic initiation, followed by dysregulation of Bcl-2 family proteins (increased BAD/BAX, decreased Bcl-2/Bcl-xl) at 12-24 hr, coinciding with mitochondrial MPTP opening and Cyt C translocation to the cytosol. Subsequent temporal activation of caspase-9 (36 hr) and caspase-3/6 (48 hr) aligned with intrinsic apoptotic signaling, while concurrent caspase-8 enhancement suggested possible extrinsic pathway involvement. Terminal events included DNA fragmentation and cytoplasmic AIF accumulation at 48 hr, though AIF nuclear translocation was not directly confirmed. Collectively, these data support FS-1 functioning as a venom-derived apoptosis-inducing agent whose activity appears coordinated through mitochondrial perturbations and caspase activation. Future validation of molecular interactions (e.g., BAD phosphorylation mechanisms, AIF subcellular trafficking) would refine this model.

ACKNOWLEDGEMENT

We thank Dr. Mark Lloyd G. Dapar, Biology Department, College of Arts and Sciences, Central Mindanao University, Musuan, Maramag, Bukidnon 8714, Philippines, for his guidance on this work.

ABBREVIATIONS

FBS: Fetal bovine serum; **IR:** Inhibition Rate; **IC_{50}:** Half-maximal inhibitory concentration; **PI:** Propidium iodide; **MPTP:** Mitochondrial Permeability Transition Pore.

CONFLICT OF INTEREST

The authors declare that there is no conflict of interest.

FUNDING

This study was supported by the Anhui Provincial Department of Education's College Student Innovation and Entrepreneurship Program (No. S202210959202 and S202210959205), Anhui Provincial Department of Education's Natural Science Foundation (No. 2023AH051713), and Domestic Study and Research Visit Grant Project for Young Key Teachers under the Teacher Training Initiative for Mid-Career and Young Teachers of the Anhui Provincial Department of Education (No. JNFX2023088).

SUMMARY

Apoptosis-associated components were isolated from*Gloydius brevicaudus* venom through sequential chromatography (DEAE-Sepharose Fast Flow anion exchange, Sp-Sepharose Fast Flow cation exchange, and Sephadex G-75 gel filtration). A tumor proliferation-inhibiting fraction, designated FS-1, displayed a single band at ~25 kDa in SDS-PAGE analysis. FS-1 treatment correlated with dose-dependent inhibition of HeLa and Hep G2 cell proliferation, showing time-responsive IC_{50} reduction with maximal effect at 48 hr. Apoptotic changes were evidenced by PS externalization detected via fluorescence staining at 6 hr. Temporal biomarker shifts included elevated BAD expression (ELISA, 12 hr) and cytosolic Cyt C accumulation coinciding with mitochondrial depletion (24 hr), alongside increased BAX and reduced Bcl-2/Bcl-xl levels. Fluorescence assays suggested MPTP opening, while caspase-8/9 activity enhancement (36 hr) preceded caspase-3/6 activation and DNA fragmentation (agarose gel electrophoresis, 48 hr). Western blot analysis of Bcl-2, Bcl-xl, caspase-3, and caspase-6 supported these observations. Cytoplasmic AIF accumulation with cleaved bands was also detected. Collectively, these findings indicate the successful isolation of FS-1-a venom protein associated with tumor cell apoptosis through mitochondrial and caspase-mediated pathways.

REFERENCES

1. Yao Xueqiang, Dong Zhen, Li Jiang, *et al.* Research progress on antibacterial activity of animal venom. Chinese Journal of Veterinary Medicine, 2024,43(03):43-7. DOI:10.13823/j.cnki.jtcvm.2024.039
2. Utkin YN. Animal venom studies: Current benefits and future developments.*World J Biol Chem*. 2015;6(2):28-33. doi:10.4331/wjbc.v6.i2.28
3. Slagboom J, Kool J, Harrison RA, Casewell NR. Haemotoxic snake venoms: their functional activity, impact on snakebite victims and pharmaceutical promise.*Br J Haematol*. 2017;177(6):947-59. doi:10.1111/bjh.14591
4. Chaisakul J, Hodgson WC, Kuruppu S, Prasongsook N. Effects of Animal Venoms and Toxins on Hallmarks of Cancer.*J Cancer*. 2016;7(11):1571-8. Published 2016 Jul 15. doi:10.7150/jca.15309
5. Xiong Yan, LI Bo, HE Qiyi, *et al.* Inhibitory Effect of *Deinagkistrodon acutus* Venom on Human Ovarian Cancer Cell Line A2780. Journal of Chongqing Normal University (Natural Science), 2019;36(5):135-40.
6. Ebrahim K, Vatanpour H, Zare A, Shirazi FH, Nakhjavani M. Anticancer Activity a of *Caspian Cobra* (*Naja naja oxiana*) snake Venom in Human Cancer Cell Lines Via Induction of Apoptosis.*Iran J Pharm Res*. 2016; 15(Suppl):101-12.
7. Moridikia A, Zargan J, Sobati H, Goodarzi HR, Hajinourmohamadi A. Anticancer and antibacterial effects of Iranian viper (*Vipera latifii*) venom; an *in vitro* study.*J Cell Physiol*. 2018;233(9):6790-7. doi:10.1002/jcp.26428
8. Gomes A, Choudhury SR, Saha A, *et al.* A heat stable protein toxin (drCT-I) from the Indian Viper (*Daboia russelli russelli*) venom having antiproliferative, cytotoxic and apoptotic activities.*Toxicon*. 2007;49(1):46-56. doi:10.1016/j.toxicon.2006.09.009
9. Duan T, Huang C H, Kong Y, *et al.* The Purification and characterization of cytotoxin from Guangxi A *Gkistrodon acutus* venom. Pharmaceutical Biotechnology, 2005;12(3):167-70.
10. Wu Y, Xu H J, Zhang X Q, *et al.* Purification and characterization of anti-tumor peptides from venom of Zhejiang *Agkistrodon acutus*. Chinese Journal of Pharmaceuticals, 2012;43(6):428-31.
11. Xu P, Zhang G B, Wang F, *et al.* Inhibitory effect of Anti-tumor component I from *Agkistrodon acutus* venom on human lung cancer A549 cells. Chinese Journal of Clinical Pharmacology and Therapeutics, 2014;19(5):493-500.
12. Yutong L, Yao S, Lihong Z, *et al. Agkistrodon acutus* venom from southern Anhui inhibiting tumor metastasis via platelets. J of Wannan Medical College, 2022;41(3):217-20.
13. Zheng M, Karki R, Vogel P, Kanneganti TD. Caspase-6 Is a Key Regulator of Innate Immunity, Inflammasome Activation, and Host Defense.*Cell*. 2020;181(3):674-87.e13. doi:10.1016/j.cell.2020.03.040
14. Chen H, Fang Z, Song M, Liu K. Mitochondrial targeted hierarchical drug delivery system based on HA-modified liposomes for cancer therapy.*Eur J Med Chem*. 2022;241:114648. doi:10.1016/j.ejmech.2022.114648
15. Xuebing P, Dongyun C, Jianguo H, *et al.* Purification of antineoplasmic activity protein from the venom of Wannan Agkistrodon and the study *in vitro*. Chin J Clin Pharmacol Ther, 2008;13(9):991-5.
16. Alghareeb SA, Alsughayyir J, Alfhili MA. Exposure to 2,4-Dichlorophenoxyacetic acid stimulates the calcium/ROS/CK1α pathway to trigger Hemolysis and Eryptosis in red blood cells.*Toxicol Res (Camb)*. 2024;13(6):tfae196. Published 2024 Nov 24. doi:10.1093/toxres/tfae196
17. Romero-Cruz VA, Ramos-Ligonio A, García-Alejandro K, Cerecedo-García M, Lagunes-Castro MS, López-Monteon A. Immunization of recombinant NS3 protein (protease region) of dengue virus induces high levels of CTLA-4 and apoptosis in splenocytes of BALB/c mice.*Virus Genes*. 2024;60(5):475-87. doi:10.1007/s11262-024-02095-2
18. Awasthi K, Huang WC, Wei CY, Hsu HY, Ohta N. Unveiling the susceptibility of nanosecond pulsed electric field on intracellular function in breast cancerous and normal cells using fluorescence imaging.*Biosens Bioelectron*. 2025;272:117129. doi:10.1016/j.bios.2025.117129
19. Voss AK, Strasser A. The essentials of developmental apoptosis.*F1000Res*. 2020;9:F1000 Faculty Rev-148. Published 2020 Feb 26. doi:10.12688/f1000research.21571.1
20. Michurina SV, Kolesnikov SI, Ishchenko IY, Bochkareva AL, Arkhipov SA. Effect of Melatonin on Expression of Apoptosis Regulator Proteins Bcl-2 and Bad in Ovarian Follicular Apparatus after High Temperature Exposure.*Bull Exp Biol Med*. 2021;170(5):598-603. doi:10.1007/s10517-021-05114-6
21. Wolf P, Schoeniger A, Edlich F. Pro-apoptotic complexes of BAX and BAK on the outer mitochondrial membrane.*Biochim Biophys Acta Mol Cell Res*. 2022;1869(10):119317. doi:10.1016/j.bbamcr.2022.119317
22. Michurina SV, Kolesnikov SI, Bochkareva AL, Ishchenko IY, Arkhipov SA. Expression of Apoptosis Regulator Proteins Bcl-2 and Bad in Rat Ovarian Follicular Apparatus during Recovery after Extreme Hypothermia.*Bull Exp Biol Med*. 2019;168(2):205-9. doi:10.1007/s10517-019-04675-x
23. Mehić B. Apoptosis - is it good or bad.*Bosn J Basic Med Sci*. 2012;12(3):1. doi:10.17305/bjbms.2012.2458
24. Rana NK, Singh P, Koch B. CoCl2 simulated hypoxia induce cell proliferation and alter the expression pattern of hypoxia associated genes involved in angiogenesis and apoptosis.*Biol Res*. 2019;52(1):12. Published 2019 Mar 15. doi:10.1186/s40659-019-0221-z

25. Yuan Z, Dewson G, Czabotar PE, Birkinshaw RW. VDAC2 and the Bcl-2 family of proteins.*Biochem Soc Trans*. 2021;49(6):2787-95. doi:10.1042/BST20210753
26. Grosser JA, Fehrman RL, Keefe D, Redmon M, Nickells RW. The effects of a mitochondrial targeted peptide (elamipretide/SS31) on BAX recruitment and activation during apoptosis.*BMC Res Notes*. 2021;14(1):198. Published 2021 May 22. doi:10.1186/s13104-021-05613-9
27. Hassan M, Watari H, AbuAlmaaty A, Ohba Y, Sakuragi N. Apoptosis and molecular targeting therapy in cancer [retracted in: Biomed Res Int. 2020; 2020:2451249. doi: 10.1155/2020/2451249.].*Biomed Res Int*. 2014;2014:150845. doi:10.1155/2014/150845
28. Willis, S., Day, C. L., Hinds, M. G., and Huang, D. C. The Bcl-2-regulated apoptotic pathway. Journal of cell science, 2003;116(20):4053-6. https://doi.org/10.1242/jcs.00754.
29. Lin, X. L., Zheng, Z. Y., Zhang, Q. S., Zhang, Z., and An, Y. Z. Expression of miR-195 and its target gene Bcl-2 in human intervertebral disc degeneration and their effects on nucleus pulposus cell apoptosis. Journal of orthopaedic surgery and research, 2021;16(1):412. https://doi.org/10.1186/s13018-021-02538-8.
30. Wang Y, Zhang Y, Sun X, Shi X, Xu S. Microplastics and di (2-ethylhexyl) phthalate synergistically induce apoptosis in mouse pancreas through the GRP78/CHOP/Bcl-2 pathway activated by oxidative stress.*Food Chem Toxicol*. 2022;167:113315. doi:10.1016/j.fct.2022.113315
31. Qi G, Yu N, Xu K, *et al.* Grass carp (*Ctenopharyngodon idella*) Bcl-xl: transcriptional regulation and anti-apoptosis analysis.*Fish Physiol Biochem*. 2020;46(2):483-500. doi:10.1007/s10695-019-00668-9
32. Vasquez-Montes V, Kyrychenko A, Vargas-Uribe M, Rodnin MV, Ladokhin AS. Conformational Switching in Bcl-xL: Enabling Non-Canonic Inhibition of Apoptosis Involves Multiple Intermediates and Lipid Interactions.*Cells*. 2020;9(3):539. Published 2020 Feb 26. doi:10.3390/cells9030539
33. Hoque MM, Iida Y, Kotani H, Kartika ID, Harada M. Hydroxychloroquine Promotes Bcl-xL Inhibition-induced Apoptosis in BxPC-3 Human Pancreatic Cancer Cells.*Anticancer Res*. 2022;42(7):3495-506. doi:10.21873/anticanres.15836
34. Morales-Martínez M, Vega MI. Roles and Regulation of Bcl-xL in Hematological Malignancies.*Int J Mol Sci*. 2022;23(4):2193. Published 2022 Feb 16. doi:10.3390/ijms23042193
35. Feng ZY, Li XR, Chen L, *et al.Zhongguo Ying Yong Sheng Li Xue Za Zhi*. 2020;36(5):385-9. doi:10.12047/j.cjap.5959.2020.082
36. Li N, Shi AM, and Liu HZ. Research Progress of Bioactive Peptides' Anticancer Function and Its Mechanism of Action. Journal of Chinese Institute of Food Science and Technology, 2019;19:267-75.
37. Pessoa J. Cytochrome c in cancer therapy and prognosis.*Biosci Rep*. 2022;42(12):BSR20222171. doi:10.1042/BSR20222171
38. Liu J, Li L, Xie P, *et al.* Sevoflurane induced neurotoxicity in neonatal mice links to a GSK3β/Drp1-dependent mitochondrial fission and apoptosis.*Free Radic Biol Med*. 2022;181:72-81. doi:10.1016/j.freeradbiomed.2022.01.031
39. Zhao P, Sun X, Chaggan C, *et al.* An AMPK-caspase-6 axis controls liver damage in nonalcoholic steatohepatitis.*Science*. 2020;367(6478):652-60. doi:10.1126/science.aay0542
40. Song L, Wang L, Hou Y, *et al.* FGF4 protects the liver from nonalcoholic fatty liver disease by activating the AMP-activated protein kinase-Caspase 6 signal axis.*Hepatology*. 2022;76(4):1105-20. doi:10.1002/hep.32404
41. Rodriguez DA, Quarato G, Liedmann S, *et al.* Caspase-8 and FADD prevent spontaneous ZBP1 expression and necroptosis.*Proc Natl Acad Sci U S A*. 2022;119(41):e2207240119. doi:10.1073/pnas.2207240119
42. Green DR. Caspase Activation and Inhibition.*Cold Spring Harb Perspect Biol*. 2022;14(8):a041020. Published 2022 Aug 1. doi:10.1101/cshperspect.a041020
43. Jiang M, Qi L, Li L, Wu Y, Song D, Li Y. Caspase-8: A key protein of cross-talk signal way in "PANoptosis" in cancer.*Int J Cancer*. 2021;149(7):1408-20. doi:10.1002/ijc.33698
44. Chen H, Zhang J, Gao Y, *et al.* Sensitive cell apoptosis assay based on caspase-3 activity detection with graphene oxide-assisted electrochemical signal amplification.*Biosens Bioelectron*. 2015;68:777-82. doi:10.1016/j.bios.2015.02.007
45. Fritsch M, Günther SD, Schwarzer R, *et al.* Caspase-8 is the molecular switch for apoptosis, necroptosis and pyroptosis.*Nature*. 2019;575(7784):683-7. doi:10.1038/s41586-019-1770-6
46. Brentnall M, Rodriguez-Menocal L, De Guevara RL, Cepero E, Boise LH. Caspase-9, caspase-3 and caspase-7 have distinct roles during intrinsic apoptosis.*BMC Cell Biol*. 2013;14:32. Published 2013 Jul 9. doi:10.1186/1471-2121-14-32
47. Wang S, Zhang Y, Gao J, Zhang J, Tao L, Xu W. The enantioselective study of the toxicity effects of chiral acetochlor in HepG2 cells.*Ecotoxicol Environ Saf*. Published online May 5, 2021. doi:10.1016/j.ecoenv.2021.112261
48. Chu H, Hou Y, Yang D, *et al.* Coronaviruses exploit a host cysteine-aspartic protease for replication.*Nature*. 2022;609(7928):785-92. doi:10.1038/s41586-022-05148-4
49. Shabanzadeh AP, D'Onofrio PM, Monnier PP, Koeberle PD. Targeting caspase-6 and caspase-8 to promote neuronal survival following ischemic stroke.*Cell Death Dis*. 2015;6(11):e1967. Published 2015 Nov 5. doi:10.1038/cddis.2015.272
50. Li Yutong, Sun Yao, Zhao Lihong, Liu Xiaoyu, and Chen Lei. Study on the inhibition of tumor metastasis through platelets by Wannan pit viper venom. Journal of Wannan Medical College, 2022;(03):217-20. doi:CNKI:SUN:WNYX.0.2022-03-004.
51. Majtnerová P, Roušar T. An overview of apoptosis assays detecting DNA fragmentation.*Mol Biol Rep*. 2018;45(5):1469-78. doi:10.1007/s11033-018-4258-9
52. Nie ZY, Yao M, Yang Z, *et al.* De-regulated STAT5A/miR-202-5p/USP15/Caspase-6 regulatory axis suppresses CML cell apoptosis and contributes to Imatinib resistance.*J Exp Clin Cancer Res*. 2020;39(1):17. Published 2020 Jan 17. doi:10.1186/s13046-019-1502-7
53. Chang Z, Yang M, Ji H. Molecular characterization and functional analysis of apoptosis-inducing factor (AIF) in palmitic acid-induced apoptosis in *Ctenopharyngodon idellus* kidney (CIK) cells.*Fish Physiol Biochem*. 2021;47(2):213-24. doi:10.1007/s10695-020-00907-4
54. Wischhof L, Scifo E, Ehninger D, Bano D. AIFM1 beyond cell death: An overview of this OXPHOS-inducing factor in mitochondrial diseases.*EBioMedicine*. 2022;83:104231. doi:10.1016/j.ebiom.2022.104231
55. Batoon L, Koh AJ, Kannan R, McCauley LK, Roca H. Caspase-9 driven murine model of selective cell apoptosis and efferocytosis.*Cell Death Dis*. 2023;14(1):58. Published 2023 Jan 24. doi:10.1038/s41419-023-05594-6
56. Su CH, Ho YC, Lee MW, *et al.* 1-Nitropyrene Induced Reactive Oxygen Species-Mediated Apoptosis in Macrophages through AIF Nuclear Translocation and AMPK/Nrf-2/HO-1 Pathway Activation.*Oxid Med Cell Longev*. 2021; 2021:9314342. Published 2021 Jul 13. doi:10.1155/2021/9314342
57. Millan, A., and Huerta, S. Apoptosis-inducing factor and colon cancer. The Journal of surgical research, 2009;151(1):163-70. https://doi.org/10.1016/j.jss.2007.05.020.

Cite this article: Hu J, Guo H, Wang C, Chen Y. Isolation and Mechanistic Exploration of FS-1: A Pro-Apoptotic Protein from Gloydius brevicaudus Venom in Tumor Cells. Indian J of Pharmaceutical Education and Research. 2026;60(4):1787-800.